(Preprint) AAS 23-116

CONSTRUCTION AND ANALYSIS OF "L_1/L_2 CYCLER" ORBITS IN THE EARTH-MOON SYSTEM

Ricardo J. Gomez[*], Juan-Pablo Almanza-Soto[*], Kathleen C. Howell[†] and Jonathan D. Aziz[‡]

As the number of missions with spacecraft in cislunar space increases, new modes of transport and space situational awareness in the Lunar vicinity are of increasing interest. This investigation introduces families of ballistic L_1/L_2 cycler orbits within the circular restricted three-body problem that continuously oscillate between the L_1/L_2 libration point regions. Subsets of these orbit families may offer coverage of the near and far sides of the Lunar surface at various elevations. These L_1/L_2 cycler orbits are validated in higher-fidelity ephemeris models and transition strategies for ensuring robustness to system sensitivities are discussed.

INTRODUCTION

The number of Lunar missions in the 2010s alone surpassed the combined total in the prior 30 years.[1] This resurgence of interest in cislunar space is multi-national and multi-faceted, reflecting the interests of various governments as well as private operators. One overarching goal is the focus for increased Space Situational Awareness (SSA) in the Lunar vicinity, motivated by the government's priority to monitor space traffic for flight safety. An implicit motivating factor behind the renewed interest is developing infrastructure that enables sustainable activity beyond Earth orbit. To this end, trajectory designers face the challenge of leveraging the non-linear gravitational field near the Moon. Periodic orbits in the vicinity of the Earth-Moon Lagrange points undoubtedly play a role in broader access to this region via their proximity to areas of interest and the potential for enabling low-cost, long-term exploration. In addition, the invariant manifolds associated with periodic orbits offer heteroclinic connections between pairs of periodic orbits, further expanding the design space for mission architectures.

Ballistic passage between the L_1 and L_2 Earth-Moon Lagrange points offers heteroclinic connections as an attractive option for mission design. Accordingly, this category of transfer is the subject of numerous research efforts. Investigations of heteroclinic connections in the planar Circular Restricted Three-Body Problem (CR3BP) date to the turn of the century, when Koon et al. demonstrated the existence of heteroclinic connections in explaining physical phenomena in the Sun-Jupiter problem.[2] Since then, analyses accomplished by Gómez et al. and Haapala and Howell extended the early work to the spatial CR3BP in multiple systems, including demonstrating ballistic connections between out-of-plane Lagrange point orbits in cislunar space.[2–4] An ongoing effort also exists in the technical community to explore this numerical problem and heteroclinic connections

[*]Ph.D. Student, School of Aeronautics and Astronautics, Purdue University, West Lafayette, IN. 47906
[†]Hsu Lo Distinguished Professor of Aeronautics and Astronautics, School of Aeronautics and Astronautics, Purdue University, West Lafayette, IN. 47906
[‡]Engineering Manager, Astrodynamics Department, The Aerospace Corporation, Colorado Springs, CO. 80916

linking L_1 and L_2 in the Earth-Moon system, including recent work by Henry and Scheeres.[5]

Previous successful efforts in constructing heteroclinic connections in the CR3BP highlight the challenges due to the dimensionality of the spatial problem. A number of authors have, however, produced specific solutions for various applications. In fact, the Themis-Artemis mission was the first spacecraft to leverage libration point trajectories and their invariant manifolds in the Earth-Moon system during 2010.[6] Notably, Haapala and Howell also demonstrate transitioning these transfers (homoclinic and heteroclinic connections) to a higher fidelity ephemeris model.[4] This investigation is focused on a particular type of transfer that demonstrates the construction of families that deliver "L_1/L_2 cycler orbits" in the Earth-Moon CR3BP; orbits that closely emulate the motion of spatial and planar heteroclinic connections. A variety of orbit geometries connecting L_1 and L_2 are constructed that closely resemble transfers between distinct known periodic orbits. In addition, transition to higher-fidelity models is addressed such that it ensures robustness to numerical sensitivities.

DYNAMICAL MODELS

This investigation leverages two different dynamical models to generate results. First, the Circular Restricted Three-Body Problem (CR3BP) is employed to construct and evaluate cycler trajectories of interest. Then, solutions are transitioned to a higher-fidelity Ephemeris model. This model employs the N-Body equations of motion to accommodate additional perturbations compared to the CR3BP.

Circular Restricted Three-Body Problem

The CR3BP is a dynamical model that accommodates the gravitational influence of two celestial bodies on a spacecraft. The mass of the spacecraft is assumed to be negligible and the primaries are assumed to follow Keplerian motion about their common barycenter. To further simplify the model, the motion of the primaries is assumed to be circular. A rotating frame is then defined with origin at the system barycenter, where the $\hat{x}$ axis is directed from the larger primary to the smaller primary, the $\hat{z}$ axis is parallel to the angular momentum vector of the orbit of the primaries, and, $\hat{y}$ completes the orthonormal triad. Figure 1(a) is a schematic of the CR3BP. The governing set of differential equations are nondimensionalized based on characteristic quantities such that the characteristic length is the distance between the primaries, the characteristic mass is the sum of the masses of the primaries, and the characteristic time is selected such that the mean motion of the system is unity. With these definitions and simplifying assumptions, the equations of motion are formulated in the rotating frame and take the form

$$\ddot{x} = 2\dot{y} + \frac{\partial U^*}{\partial x}, \quad \ddot{y} = -2\dot{x} + \frac{\partial U^*}{\partial y}, \quad \ddot{z} = \frac{\partial U^*}{\partial z} \tag{1}$$

where the coordinates (x, y, z) and $(\dot{x}, \dot{y}, \dot{z})$ correspond to positions and velocities, respectively, measured in the rotating frame. The quantity U^* represents a pseudo-potential function defined as

$$U^* = \frac{1}{2}(x^2 + y^2) + \frac{1-\mu}{r_{13}} + \frac{\mu}{r_{23}} \tag{2}$$

where r_{13} and r_{23} represent the distances from the spacecraft to the larger and smaller primaries, respectively, and μ is the nondimensional mass of the smaller primary (also known as the characteristic parameter of the system), defined as $\mu = m_2/(m_1 + m_2)$. The equations of motion in this

model are autonomous. The differential equations also possess an integral of the motion, i.e., the Jacobi constant. This energy-like quantity is defined in terms of the magnitude of the spacecraft rotating velocity v and the pseudo-potential function, as $JC = 2U^* - v^2$, where $v = \sqrt{\dot{x}^2 + \dot{y}^2 + \dot{z}^2}$. Periodic orbits and transfer solutions exist over a wide range of energies in this model, hence, evaluating the range of Jacobi constant over a family provides insight into the breadth of available solutions.

Higher-Fidelity Ephemeris Model

In addition to characteristics of L_1/L_2 cycler orbit families in the CR3BP, this investigation also addresses the behavior of these orbits in a higher-fidelity model. Although the CR3BP is a practical platform for trajectory design and analysis, the dynamics do not incorporate all perturbations inherent to the motion of the system. These additional forces may be significant and necessitate non-trivial numerical strategies for transitioning CR3BP trajectories to their higher-fidelity counterparts. To investigate these challenges, a higher-fidelity ephemeris model is defined by incorporating planetary ephemerides into the N-body equation of motion. The N-body relative equations of motion describe the trajectory of a mass-less particle $P_{s/c}$ with respect to a gravitational central body P_j. The remaining $N-2$ bodies, denoted P_i, contribute gravitational perturbations as governed by the vector expression

$$\frac{d^2\boldsymbol{r}_{s/c,j}}{dt^2} = G\frac{m_j}{r_{s/c,j}^3}\boldsymbol{r}_{s/c,j} + G\sum_{\substack{i=1 \\ i\neq j,s/c}}^{N} m_i\left(\frac{\boldsymbol{r}_{s/c,i}}{r_{s/c,i}^3} - \frac{\boldsymbol{r}_{j,i}}{r_{j,i}^3}\right) \tag{3}$$

where G is the universal gravitational constant, $\boldsymbol{r}_{i,j}$ is the position vector of mass i relative to j, m_α is the mass of particle P_α, and t represents epoch. Figure 1(b) is a schematic of the ephemeris model. In contrast to Equation (1), Equation (3) is non-autonomous and formulated in a body-centered inertial frame coinciding with the central mass m_j. This investigation employs the Moon-centered ecliptic J2000 frame; the coordinate transformation to the barycentric CR3BP frame is described by previous authors.[7] The gravitational influences of the Earth, Moon and Sun are sufficient for describing spacecraft motion in cislunar space and their ephemerides are sourced from the DE440 data set published by the Jet Propulsion Laboratory.[8–10]

PERIODIC ORBITS IN THE CR3BP

While no general analytical solution for motion in the CR3BP is available, periodic solutions relative to both the primaries and the equilibrium points of the system exist, providing repeatable solutions that are useful for mission design. In the CR3BP, periodic solutions exist in families that progress across various energy levels. For reference, subsets of periodic orbits in the Lyapunov, halo, and Direct Prograde Orbit (DPO) families are plotted in Figure 2; as they are referenced throughout this analysis. Note that these orbit families are all symmetric across the x-z plane, a property that is leveraged for periodic construction of individual orbits in this investigation. Additionally, periodic orbit families can be represented many ways, including a period-JC hodograph to more easily compare the ranges in energy and period over each family. Such a hodograph is displayed in Figure 3. The stability of periodic orbits varies in this model. The linear stability of a periodic orbit is defined via the associated monodromy matrix (i.e., the state transition matrix after precisely one period of the orbit). If at least one eigenvalue possesses a magnitude larger than 1, the periodic orbit is unstable. In these families, the eigenvalues evaluated from the monodromy matrix exist

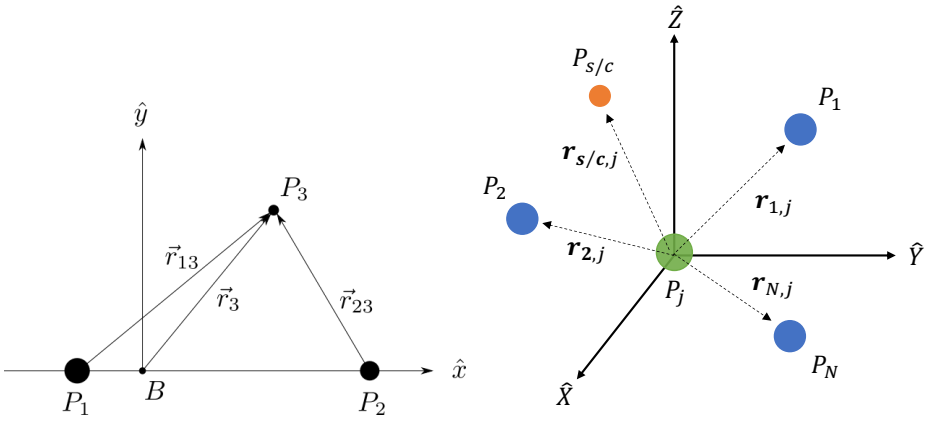

Figure 1: (a) CR3BP rotating frame (b) Schematic of N-body ephemeris model.

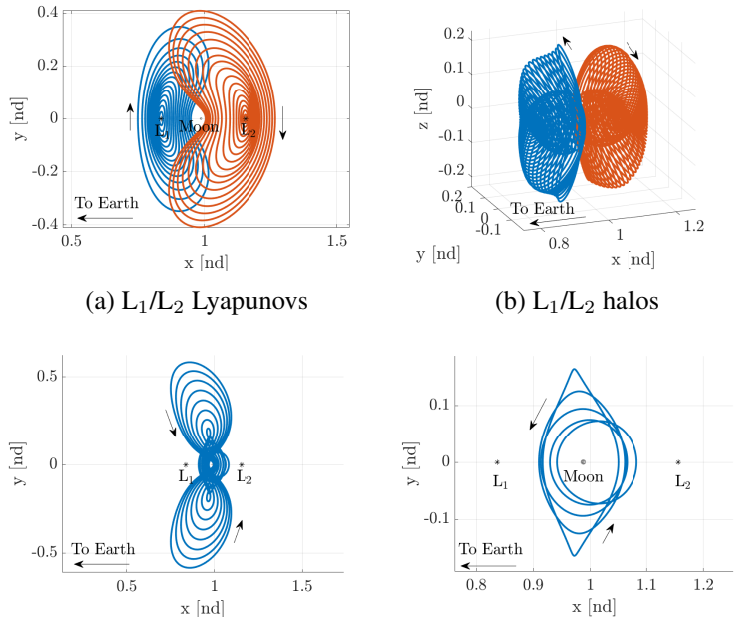

Figure 2: Sample orbit families in the CR3BP; viewed in the rotating frame with origin at the system barycenter

in reciprocal pairs. If an orbit is unstable, then, due to the reciprocal nature of the eigenvalue pairs, such orbit has stable and unstable manifolds associated with it; these are natural structures that provide free arrival and departure options, respectively. The range of interest in the Lyapunov families of orbits are unstable, and a sample L_1 orbit and its corresponding manifolds are plotted in Figure 4, where the trajectories along the stable manifold are colored in blue and trajectories along the unstable manifold are colored in red. If a stable manifold trajectory arc intersects an unstable manifold trajectory arc that corresponds to the same orbit, in position and velocity space,

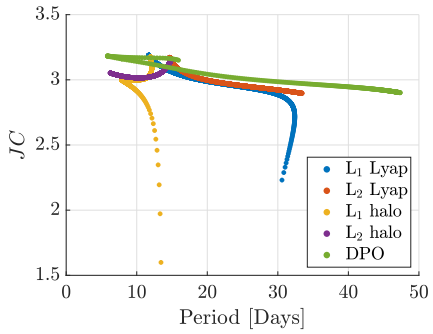

Figure 3: Hodograph of sample orbit families in the CR3BP

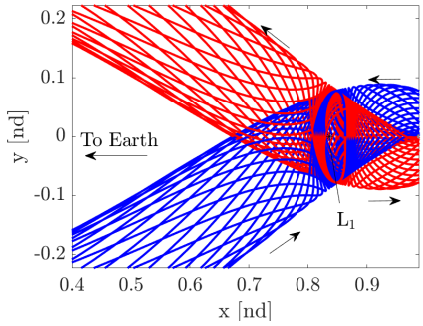

Figure 4: Manifolds of L_1 Lyapunov (stable trajectories in blue and unstable trajectories in red)

a free excursion away from and returning to the orbit is available, and is denoted a homoclinic connection. In contrast, if an unstable manifold trajectory arc from one orbit intersects a stable manifold trajectory arc corresponding to a different orbit in full state, a free transfer between those orbits exists, and is labelled a heteroclinic connection.

HETEROCLINIC CONNECTIONS IN THE CR3BP

Heteroclinic connections provide maneuver-free transfers between periodic orbits at the same energy level in the CR3BP. Previous authors demonstrate the existence of heteroclinic connections between L_1/L_2 Lyapunov orbits over a wide range of energy levels.[4,11,12]

For simplicity, the analysis first considers solutions in the Earth-Moon plane by recreating such free transfers. Potential heteroclinic transfers are identified by propagating the manifold trajectories of L_1/L_2 Lyapunov orbits until they intersect a hyperplane defined at the x location of the Moon. Note that construction of manifold trajectories in this analysis all employ a step-off value of 50 km. The intersections of the manifold trajectories with this hyperplane are visualized on a map characterized by their y position and velocity (v_y), where the pair of sampled points with the smallest discrepancy is then selected as the initial guess for the corrections process. For this study, the smallest discrepancy is defined as the minimum difference in the norm of the difference of the y and v_y values at the hyperplane. This process is visualized for a sample set of orbits in Figure 5. The methodology as detailed by Haapala,[4] is then leveraged in a corrections process to adjust the initial guess into a free transfer. This sample scenario only considers the first return to the hyperplane, however, additional returns can be incorporated to uncover a variety transfer structures.

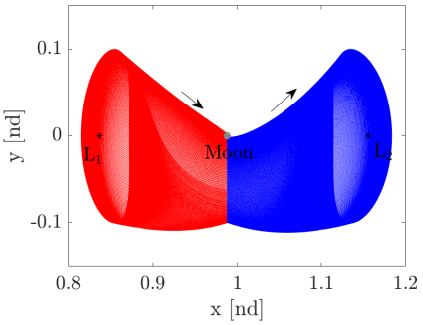

(a) Lyapunov orbits and their manifold trajectory arcs (unstable from L_1 in red, stable from L_2 in blue) in Earth-Moon CR3BP

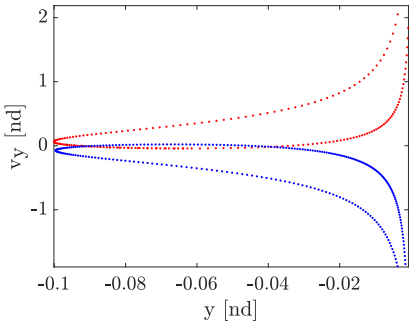

(b) Map of manifold trajectory arc intersections at $x = 1 - \mu$ hyperplane

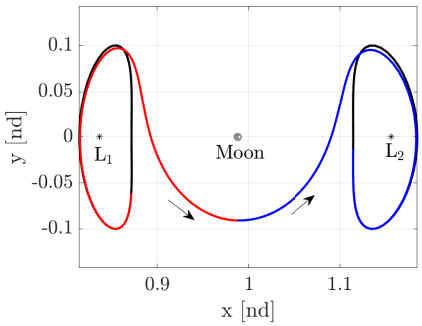

(c) Initial guess identified from map (unstable manifold trajectory in red, stable manifold trajectory in blue, orbits in black)

Figure 5: Planar heteroclinic connection initial guess generation process in Earth-Moon CR3BP

These transfers with potentially multiple revolutions of the smaller primary have previously been examined for libration point missions.[13] Figure 6 illustrates transfers available when varying the number of returns to the hyperplane. Also notable, in the Earth-Moon system, the transfers appear

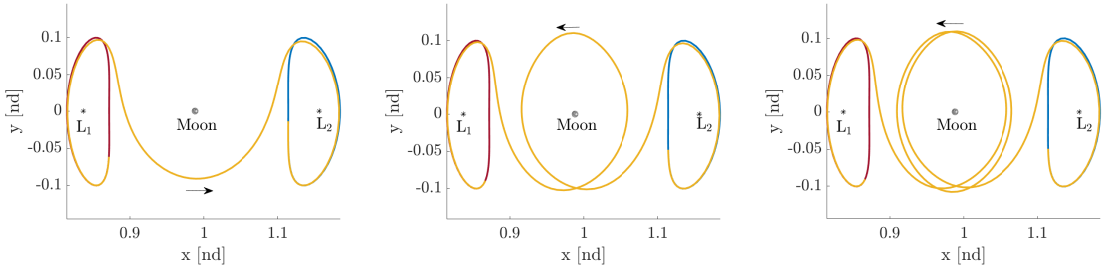

Figure 6: L_1/L_2 Lyapunov heteroclinic connections in Earth-Moon CR3BP (Initial orbit in red, transfer arc in yellow, final orbit in blue)

to transit along a DPO on their way across cislunar space[11] (notice the similar structures between Figures 6 and 2(d)). To verify, an unstable DPO at this energy level is directly incorporated into the transfer trajectory by computing a two-step transfer, where the first leg is a heteroclinic connection from an L_1 Lyapunov to a DPO at the same energy level, and the second leg is a heteroclinic connection from the selected DPO to an L_2 Lyapunov also at the selected energy level. The two segments are blended to deliver a transfer. This two-step transfer is then visualized along with the directly-generated 3-map-return transfer between the same L_1/L_2 Lyapunov pair in Figure 7. Both

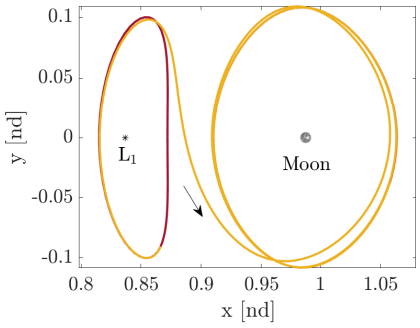

(a) L_1 Lyapunov to DPO heteroclinic connection

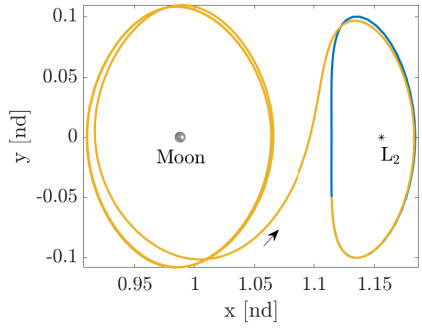

(b) DPO to L_2 Lyapunov heteroclinic connection

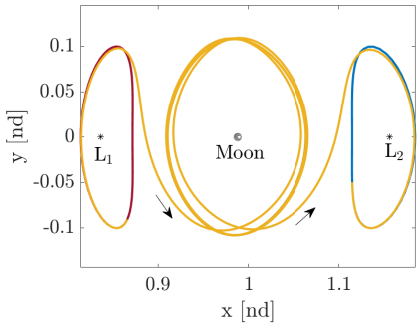

(c) Overlaid two-legged transfer

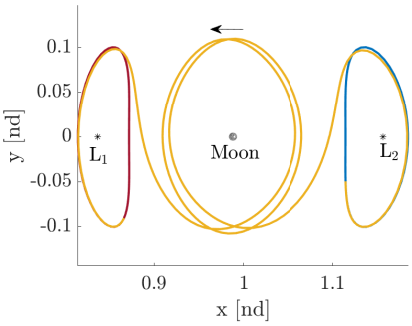

(d) Directly computed transfer

Figure 7: Comparison of Lyapunov heteroclinic transfer directly/indirectly leveraging DPO in the Earth-Moon CR3BP (Initial orbit in red, transfer arc in yellow, final orbit in blue)

the directly and indirectly computed transfers are visually identical, highlighting that the L_1/L_2 Lyapunov heteroclinic transfer geometries apparently exploit the underlying structures from DPOs, as discussed by Vaquero.[11] Next, continuation techniques are implemented to generate families of transfer solutions from L_1 Lyapunov orbits to L_2 Lyapunov orbits at the corresponding energy levels, appearing in Figure 8. The families in this figure utilize underlying structures i.e., manifolds, that belong to orbits from the DPO family, across the section of the family in the figure. Hence, these families of heteroclinic connections only exist in the energy range over which the DPOs are unstable.[11] To support this claim, Figure 9 presents a hodograph, where these transfer families are overlaid on a hodograph of the DPO family, with stable orbits colored in black and unstable orbits in red. Notice how a majority of the included DPO family is unstable, with a small range where the orbits in this family are stable. Note that the energy range over which the computed heteroclinic families exist is exclusively limited within the energy range in which the DPO family is unstable,

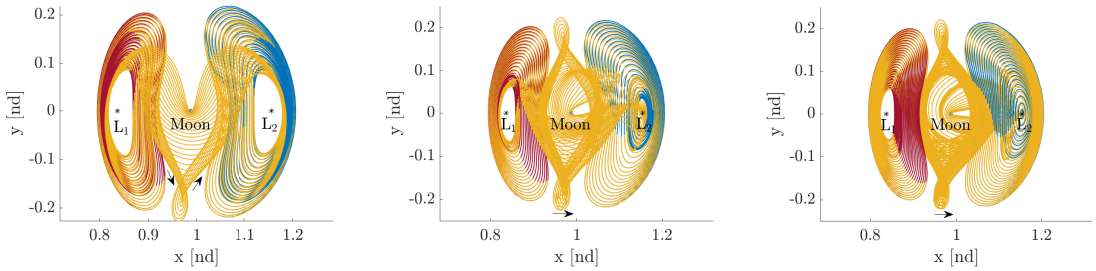

Figure 8: Families L_1/L_2 Lyapunov of heteroclinic connections in Earth-Moon CR3BP (Initial orbits in red, transfer arcs in yellow, final orbits in blue)

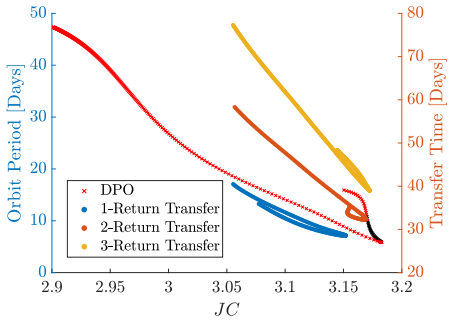

Figure 9: Hodograph comparisons of DPO family of orbits and the L_1/L_2 Lyapunov heteroclinic families

as expected. Finally, note that heteroclinic connections are not limited to the Earth-Moon plane, as they also exist in the spatial CR3BP.[4] However, spatial heteroclinic connections are significantly more challenging to identify and construct, and, due to the dimensionality of the problem, they do not exist in families when connecting pairs of periodic orbits as the solutions in the planar problem do. Due to the inherent complexities, spatial heteroclinic transfers are not directly constructed in this investigation, but it is not necessary here. Nonetheless, previous authors have identified select solutions between various spatial families of periodic orbits in cislunar space.[4]

CISLUNAR L_1/L_2 CYCLER TRAJECTORIES

Periodic orbits that continuously transit various locations of cislunar space are of particular interest as they present a myriad of potential science and situational awareness applications. In this analysis, heteroclinic transfers are transformed into periodic L_1/L_2 cycler trajectories, such that traditional periodic orbit family techniques are leveraged to expand the solution space. The techniques leveraged to generate these L_1/L_2 cycler trajectories are summarized here, along with the numerical challenges highlighted, and alternative augmentation techniques identified to overcome the challenges.

Construction of Cycler Trajectories

In the CR3BP, there exists a mirror configuration, such that trajectories reflected across the x-z plane are symmetric when propagated in backwards time.[14] This property is often leveraged in periodic orbit construction by employing perpendicular crossings across the plane of symmetry.

Due to this property, heteroclinic connections between L_1/L_2 Lyapunov orbits occur in symmetric pairs; that is, a heteroclinic transfer from an L_1 Lyapunov to an L_2 Lyapunov orbit is the mirror image of a heteroclinic transfer from an L_2 Lyapunov to an L_1 Lyapunov periodic orbit.[5] Figure 10 illustrates this property for a set of Lyapunov orbits at a specified value of JC. This symmetric

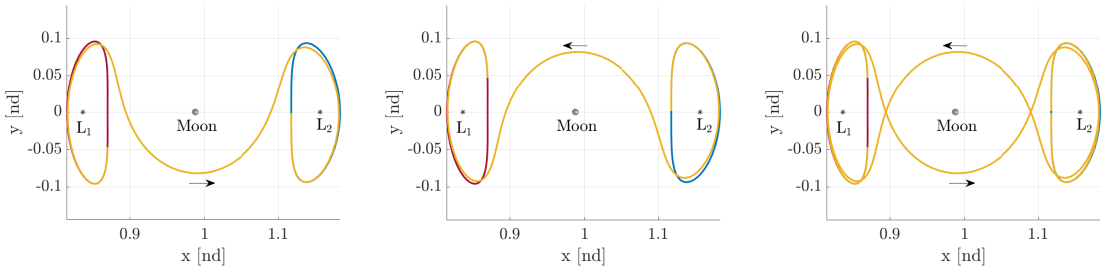

(a) L_1 to L_2 Lyapunov transfer (b) L_2 to L_1 Lyapunov transfer (c) Heteroclinic cycle

Figure 10: Sample heteroclinic cycle in Earth-Moon CR3BP

property extends to any heteroclinic transfer between orbits that possess this mirror configuration. Koon et al. previously investigated chaining these symmetric pairs, denoted heteroclinic cycles, along with homoclinic connections to produce system tours.[2] The underlying structures from these maneuver-free transfers are leveraged to construct new planar periodic orbits denoted "L_1/L_2 cycler" trajectories. To transform the heteroclinic cycle into a periodic orbit, segments of the underlying orbits and the transfer arc are chained together to arrive at a fully periodic solution. The steps in the construction process involve all of the dynamical structures available as follows. (i) Originating on the transfer arc, corresponding to the x position of the Moon, the trajectory is propagated towards each orbit, until the first crossing of the x-z plane after arrival, as illustrated in Figure 11. In this

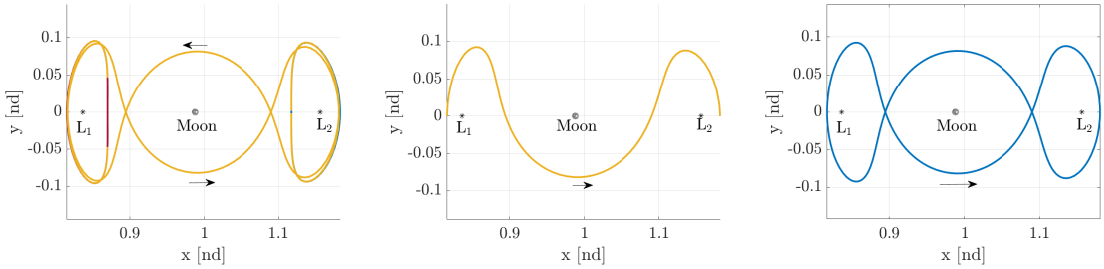

(a) Initially selected transfer (b) Periodic cycler initial guess (c) Corrected solution

Figure 11: Corrections problem visualization

example, arrival is defined as the time that the transfer arc crosses the x location corresponding to each equilibrium point, assuming that the arriving transfer arc closely matches the corresponding Lyapunov structure. Arrival may also intuitively be defined as the location at which the manifold step-off occurs, but such a definition may lead to longer TOFs for the cycler trajectory depending on the stability, such a scenario also potentially presents numerical challenges. (ii) A numerical corrections method is then employed to ensure perpendicular crossings at the x-z plane intersection at each end point, while maintaining continuity along the trajectory; leading to a single revolution of a corrected L_1/L_2 cycler periodic trajectory.

Once a periodic orbit is generated via a chaining scheme, a continuation scheme is leveraged to compute a family of such planar periodic cycler trajectories. A representative set of members in this family appear in Figure 12. The exterior lobes of the orbit shown in Figure 12(c) visually resemble L_1/L_2 Lyapunov orbits. The interior lobe resembles a DPO, most obviously apparent in Figures 12(b) and 12(c), a characteristic of many L_1/L_2 Lyapunov heteroclinic connections.[11] The gener-

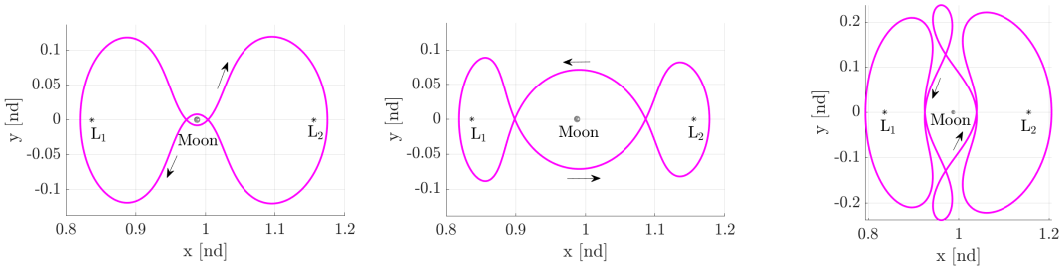

(a) $JC = 3.108$, $\mathcal{P} = 20.33$ Days (b) $JC = 3.151$, $\mathcal{P} = 30.56$ Days (c) $JC = 3.050$, $\mathcal{P} = 51.62$ Days

Figure 12: Sample planar L_1/L_2 cycler trajectories; each plot includes one period of the cycler

ated family of planar L_1/L_2 cycler orbits is then represented on a hodograph along with the DPO family in Figure 13, where the cycler family is visualized using circle markers and the DPO family is denoted with 'x' markers. Additionally, the members of these families are colored by their stability properties, where a red marker represents an unstable orbit, and a black marker identifies a stable orbit. Note that in this case, the energy range in which family of planar L_1/L_2 cycler trajectories exists extends beyond the energy range in which the DPO family is unstable. This result is in contrast to the families of heteroclinic transfers shown in Figure 9, which were limited to the energy range in which the DPO family is unstable. While the planar cyclers are constructed leveraging structures from heteroclinic transfer, they expand the available energy range of the solution space beyond the range in which DPO manifolds are available. Next, a bifurcation analysis is useful for the cycler

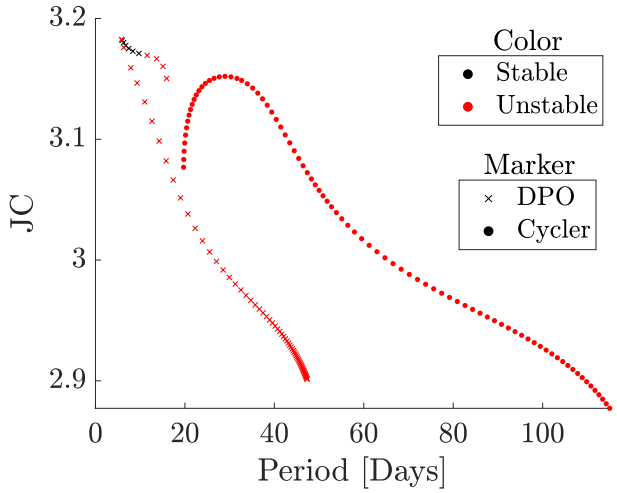

Figure 13: Planar L_1/L_2 cycler trajectories hodograph overlaid with DPO family (cycler represented by circles, DPO by 'x' marker)(Unstable orbits in red, stable in black)

family to evaluate possible links with other periodic orbit families in their vicinity. A Broucke stability diagram[15] approach is implemented in this investigation to identify the bifurcating orbits. For this family, four tangent bifurcations, a cyclic fold bifurcation and five period doubling bifurcations are identified and marked on the period-JC hodograph on Figure 14, where the red markers represent tangent bifurcations, the black markers locate period doubling bifurcations, and the green marker (at the maximal JC level) represents the cyclic fold. Once bifurcations are identified, some

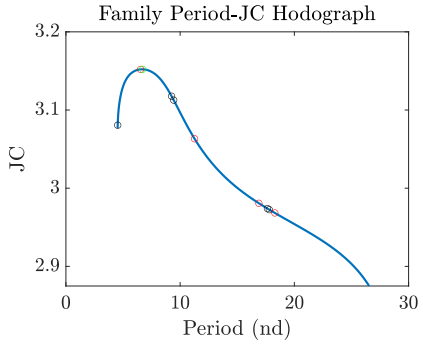

Figure 14: Planar L_1/L_2 cycler trajectories bifurcation analysis (tangent bifurcations circled in red, cyclic fold in green and period doubling in black)

bifurcating periodic orbit families are constructed when appropriate. Note that the bifurcation at the maximum JC value (cyclic fold) does not yield a new family. To generate the periodic orbit families that bifurcate from the planar L_1/L_2 cycler family, the null space information for the Jacobian from the periodic orbit targeting problem is leveraged, as detailed by Zimovan-Spreen.[16] This targeting strategy is selected as it provides an updated initial guess for every free variable in the targeting problem, useful in multiple shooting scenarios. Taking the first tangent bifurcation as an example (the bifurcating orbit with the shortest period, marked by the leftmost red circle), the out-of-plane eigenvectors serve as the basis for a new spatial family. A new family of spatial L_1/L_2 cycler trajectories is generated and its characteristics are overlaid on a hodograph, along with those of the planar family, as displayed in Figure 15, where the orange line represents the spatial family, and the blue line reflects the planar family. Note that the orange curve is a single continuous line that has multiple members at certain energy levels and visually appears to overlap itself. This new family introduces a large range of periodic orbits that possess orbit-to-orbit transfer-like structures. Some sample orbits from this spatial family are plotted in Figure 16. The individual orbits are labelled with the structures that are visually apparent.

As solutions that traverse the near-Moon region are of particular interest, the section of the spatial L_1/L_2 cycler family that incorporates halo-to-halo transfer structures is isolated. This subsection of the family, along with a few representative individual members are displayed in Figure 17. Notice that this isolated part of the family provides a continuous evolution of L_1/L_2 cycler trajectories originating from the planar case and the Lyapunov orbit families, expanding out-of-plane, to the halo families, including the various geometries available in the halo family.

Heteroclinic connections between L_1/L_2 three-dimensional halo orbits in the spatial problem are challenging to locate numerically, and are not always predictable to locate.[4] In contrast, the methodology exploited in this investigation allows for the construction of spatial L_1/L_2 cycler trajectories that yield families of periodic orbits that may encompass a range of structures reflecting other types of transfers, thereby providing innovative strategies to traverse the Lunar vicinity.

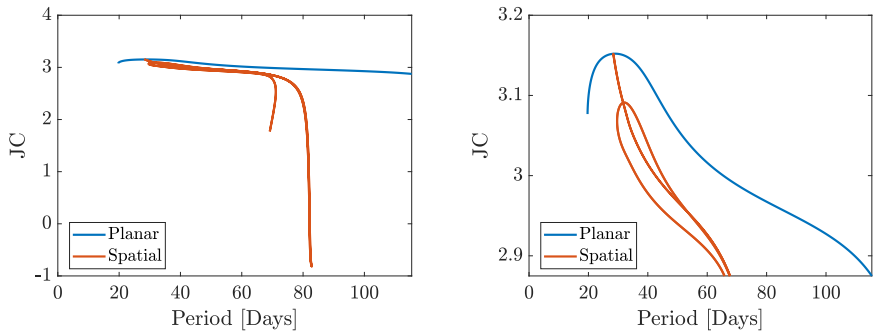

Figure 15: Hodograph representation of the planar and Spatial L_1/L_2 cycler families

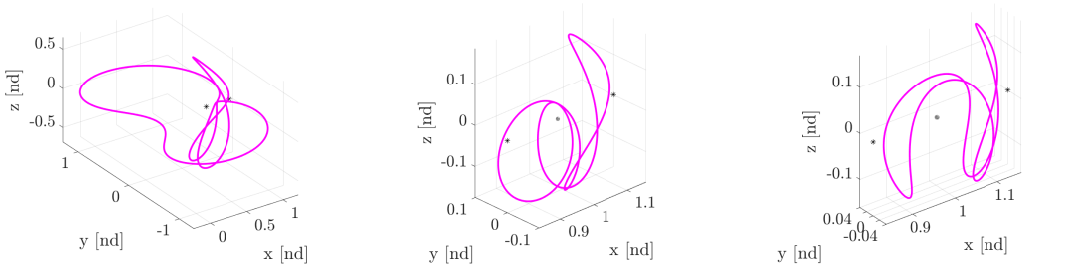

(a) L_1 Lyapunov to L_2 Vertical (b) L_1 Halo to L_2 Vertical (c) Butterfly to L_2 Vertical

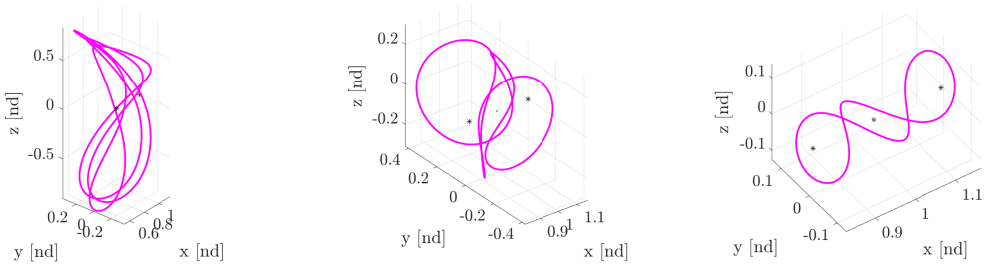

(d) L_1 Vertical to L_2 Vertical (e) L_1 P2HO2 to L_2 Vertical (f) L_1 Halo to L_2 Halo

Figure 16: Sample spatial L_1/L_2 cycler trajectories that reflect a wide range of characteristics

Cycler Augmentation and Numerical Challenges

The L_1/L_2 cycler trajectories from the previous section possess a single revolution around each equilibrium point as they transit across the cislunar region. However, the methodology also allows for the inclusion of extended time in the vicinity of either equilibrium point. During the construction and in the formulation of the targeting problem for these orbits, the transfer arc is propagated until the first crossing of the x-z plane after arrival. As an alternative, assume that a second plane crossing is included on each end as part of the initial guess, i.e., an additional revolution in the vicinity of the end point orbits is incorporated in the final corrected cycler orbit. With this procedure, cycler trajectories are augmented to spend an increased interval in the regions of interest. This augmentation need not be symmetrical, that is, different numbers of revolutions are potentially incorporated in the vicinity of either equilibrium point. A demonstration of the discussed augmentation is offered

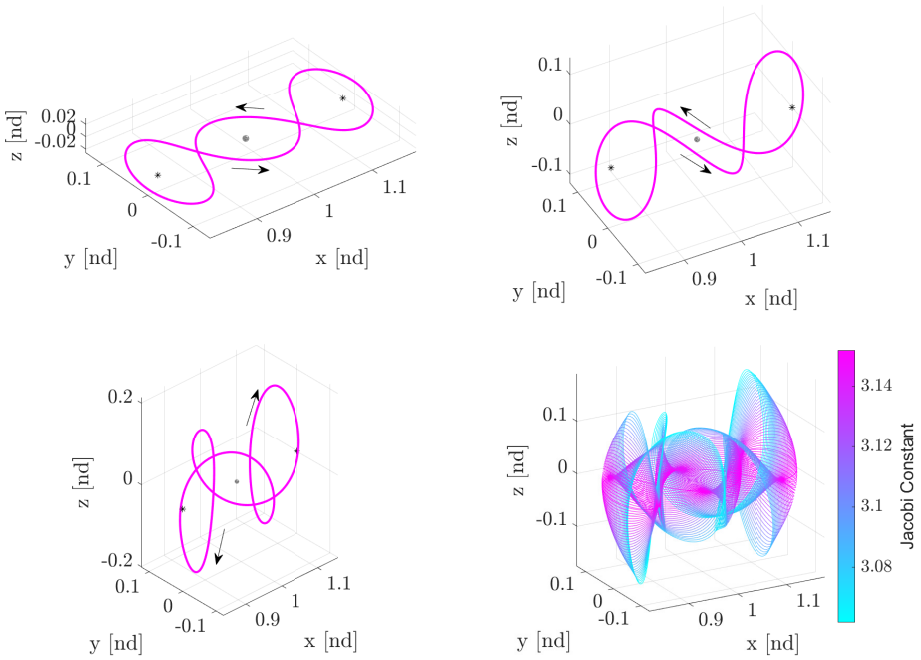

Figure 17: Sample spatial L_1/L_2 cycler trajectories that display structures consistent with halo-to-halo transfers

in Figure 18.

Including these additional revolutions, not surprisingly, introduces numerical challenges when assessing the stability properties for these orbits. Due to the extended time-of-flight along these types of orbits, eigenvalues of the monodromy matrix grow substantially larger, adding significant numerical challenges for accurate monodromy matrix computations. These challenges can prevent identification of bifurcating orbits in these augmented orbit families and, subsequently, computation of adequate initial guesses for families in their vicinity. Note that these challenges do not immediately hinder continuation for families of periodic orbits, so, families of augmented cycler trajectories are still straightforwardly constructed. Due to the inability to compute the bifurcating orbits, generation of augmented spatial cycler families cannot be achieved using the same methodology. To overcome the numerical difficulties, an alternative augmentation scheme is devised. Rather than continuing from the planar problem, the alternative scheme attempts to directly augment the spatial counterparts. First, a target spatial cycler is selected for augmentation. Next, halo orbits in its vicinity are selected by identifying the orbit with the most similar perpendicular crossing in position space (evaluated using the Euclidean norm of the difference in x and z positions at the perpendicular crossing). Finally, a targeting problem is created to chain the desired number of extra revolutions on each end with half of the specified spatial cycler, enforcing perpendicular crossing constraints at the end for the halo orbit that serves as the basis for the additional revolutions. Continuity between the halo orbits and the cycler are also enforced during the convergence process. As the targeting problem iteratively seeks a solution, an augmented spatial cycler emerges, such as the example plotted in Figure 19. Given a single solution, traditional continuation methods are employed to generate a family of augmented spatial solutions.

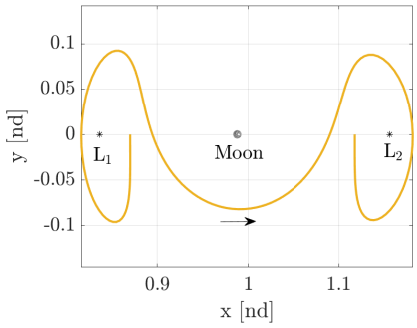

(a) Initial guess

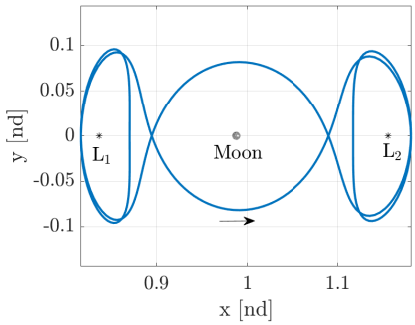

(b) Corrected cycler with 2 revolutions in the vicinity of both L_1/L_2

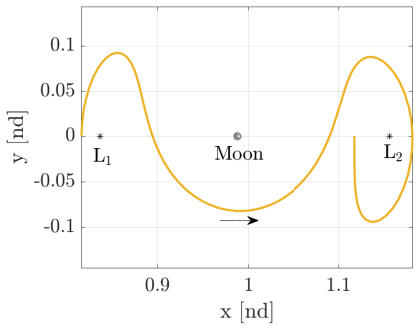

(c) Initial guess

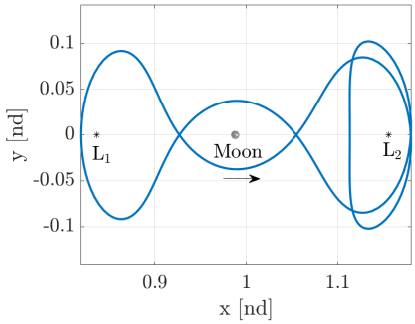

(d) Corrected cycler with one revolution near L_1 and two revolutions in the vicinity of L_2

Figure 18: Augmented planar L_1/L_2 cycler trajectories with one or more revolutions specified near each libration point

TRANSITION TO HIGHER-FIDELITY EPHEMERIS MODEL

The cycler orbits constructed in the Earth-Moon CR3BP are transitioned to a higher-fidelity ephemeris model. The transition strategy is aimed at preserving the solution geometry originally produced in the CR3BP. Although the periodic behavior of the cycler trajectories is coupled to both the circular-restricted assumption and, in general, the rotating frame, the N-body equations of motion often admit quasi-periodic solutions possessing similar geometric characteristics. Several authors successfully transition libration point orbits from the CR3BP to ephemeris models using a stacking strategy.[4,13,17,18] In this approach, multiple revolutions of a periodic orbit in the CR3BP are discretized then propagated in the higher-fidelity model. The resulting position and velocity discontinuities are removed using a standard differential corrections scheme. At some computational expense, the inclusion of several revolutions of the initial guess biases the corrections algorithm toward quasi-periodic motion, analogous to that of the underlying CR3BP orbit. This stacking strategy is applied here to produce long-term L_1/L_2 cycler trajectories in a Sun-Earth-Moon (SEM) ephemeris model.

Long-term ephemeris solutions that maintain their geometry demonstrate robustness to time-dependent perturbations that are not represented in the CR3BP. One such cycler trajectory is plotted

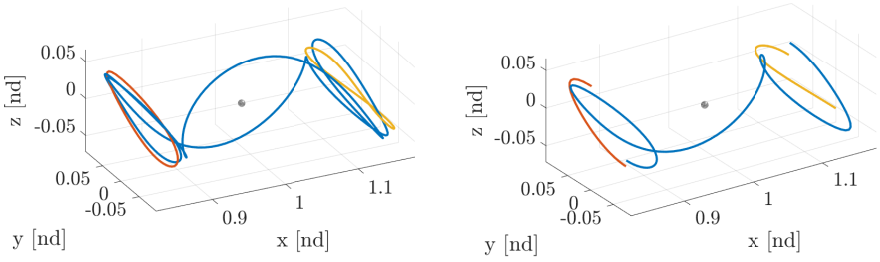

(a) Selected orbits

(b) Initial guess

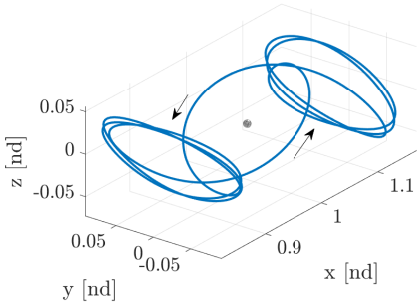

(c) Corrected cycler

Figure 19: Sample augmented spatial L_1/L_2 cycler trajectory

in Figure 20; here the CR3BP initial guess is plotted alongside an ephemeris counterpart with a three-year time-of-flight. The representation in the rotating frame highlights the qualitative geometric similarities between the orbits. In particular, the distinct lobes on the near and far sides of the Moon as well as symmetry across the x-z plane are approximately preserved in the ephemeris transition. Note that the rotating states in Figure 20(b) are non-dimensionalized by the instantaneous Earth-Moon distance such that the dimensional value along any axis direction varies as the states evolve over the trajectory. Table 1 provides a quantitative comparison of some parameters in Figure 20. The quasi-periodic motion along the ephemeris trajectory varies non-uniformly in comparison with the underlying CR3BP orbit; the degree of the maximum variation is encompassed by the perilune and out of plane excursion metrics. It is noted that, while the relative change in minimum perilune pass is significantly larger than for the maximum z-excursion, neither metric is constrained during the corrections process. These constraints may be incorporated for various applications. The other metric, mean period, offers a comparison of changes in average speed across the three-year propagation. Note that the 'period' for the ephemeris trajectory is defined as the time between passes of the x-z plane such that $x < 1 - \mu$ and $z > 0$. By this measure, the ephemeris orbit closely retains the period of the CR3BP initial guess, despite there being no constraints on the time-of-flight.

The direct orbit stacking strategy is effective and robust in transitioning cycler orbits to ephemeris models. However, the particular implementation of the corrections algorithm may exacerbate numerical sensitivities to other variables in the system, such as the initial epoch. For example, the halo-to-halo cycler orbit geometry in Figure 20(a) is well-preserved employing a simple transi-

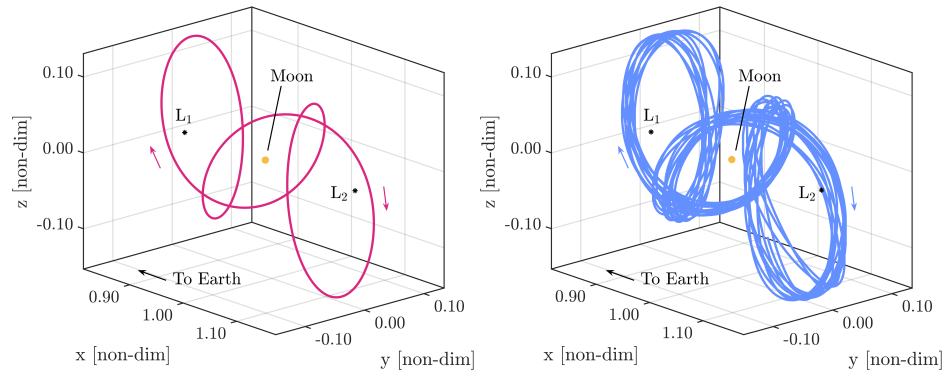

Figure 20: Comparison of (a) CR3BP L_1/L_2 cycler orbit and (b) the corrected, three-year, counterpart in an SEM ephemeris model. The ephemeris trajectory in Figure 20(b) is represented in a rotating frame with origin at the instantaneous barycenter of the Earth and Moon and possesses an initial epoch of Jan. 1 2023 00:00:00 UTC.

Table 1: Comparison of CR3BP cycler and ephemeris trajectories in Figure 20.

Model	Min. Perilune	Max. z-Excursion	Mean Period
CR3BP	3.6771e+04 km	4.9800e+04 km	31.0769 days
SEM Ephemeris	2.8167e+04 km	5.3133e+04 km	31.0827 days
% relative change	23.40	6.693	0.0149

tion algorithm at the specified initial epoch. This behavior is not guaranteed to generalize to other epochs, however, as illustrated by the plot in Figure 21. This trajectory is produced from the CR3BP initial guess in Figure 20(a) and leverages the same corrections algorithm resulting in Figure 20(b), but fails to retain the geometry apparent in the initial guess, particularly the lack of retaining the out-of-plane amplitude. Importantly, variations in ephemeris solution geometry constructed from a common initial guess with small changes in some parameters, e.g., epoch, may not necessarily reflect changes in system dynamics; rather, the varying behaviors potentially indicate a need to adjust the numerical algorithm. In such scenarios, intermediate numerical models provide valuable insights for determining first, if an acceptable ephemeris analog exists at the desired epoch, and second, the necessary adjustments to the transition strategy.

Previous investigations regarding the ephemeris equations of motion suggest that differences between cycler orbit geometry in the CR3BP and the characteristics in an ephemeris model are more likely governed by the pulsating distance between the Earth and Moon for trajectories in the L_1/L_2 vicinity.[17] This specific perturbation is analyzed in isolation utilizing an elliptical-restricted three-body model (ER3BP) that describes the relative motion of the Earth and Moon as elliptical rather than circular. In this non-autonomous model, the CR3BP halo-to-halo cycler orbit possesses the Quasi-Periodic Orbit (QPO) counterpart plotted in Figure 22. The ER3BP orbit is robust to changes in epoch and closely resembles the ephemeris cycler in Figure 20(b), suggesting that ephemeris counterparts preserving this geometry are also available at other epochs when the appropriate numerical strategy is employed. It is observed that phasing challenges do add to the complexity when

incorporating the ER3BP.

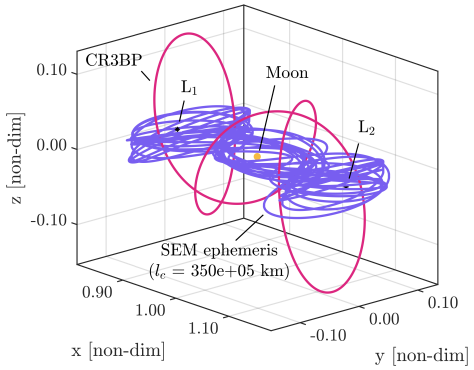

Figure 21: Collapsing behavior during an iterative corrections process in the ephemeris model resulting from numerical sensitivities. Initial epoch Jan. 20 2023 00:00:00 UTC.

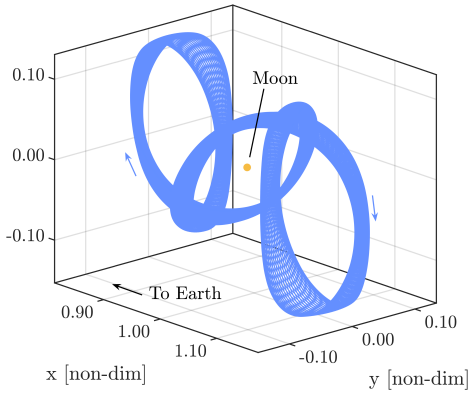

Figure 22: Quasi-periodic orbit in the elliptical restricted three-body problem generated from the CR3BP initial guess in Figure 20(a). Note the close resemblance to the ephemeris counterpart Figure 20(b). [Computation by Beom Park].

Changes in characteristic parameters, those incorporated in the non-dimensionalization of the ephemeris equations of motion, actually function as tuning parameters for the ephemeris corrections process. This sensitivity occurs because changes in the characteristic length l_c and time t_c influence the state propagation and, thus, alter the solution result from the correction process. Note that, for any ephemeris propagation, the characteristic time is defined as $t_c = \sqrt{l_c^3/(G(m_1 + m_2))}$ as in the CR3BP. The sensitivity of the corrections process to the values of l_c and t_c are then exploited such that the result of the ephemeris transition process corresponds to the initial guess by a selected metric, or a combination of metrics as illustrated in Figure 23. In this figure, percent relative changes in the metrics from Table 1 are evaluated as a function of the characteristic parameter l_c. Each set of points at a fixed l_c value is evaluated from a single ephemeris cycler orbit. The value of each point along the vertical axis indicates the degree that a particular metric is preserved in the transition process from the CR3BP to the ephemeris model for a specific epoch date. Moreover, large values in the plot represent a failure to retain a desirable geometric characteristic while small values indicate better geometry retention. The trends in the plot delineate a region of values for l_c that outperform others under these metrics, denoted "ideal l_c region" in Figure 23. A value for

l_c = 3.84e+05 km, for example, is selected to ensure geometry retention at this epoch. Note that comparisons of these specific ephemeris trajectories to the ER3BP QPO lead to approximately the same ideal values for l_c.

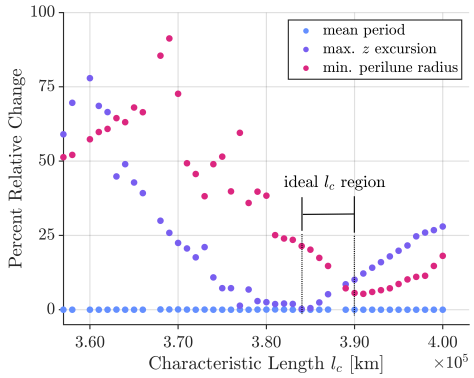

Figure 23: Measured changes in solution geometry between CR3BP and SEM ephemeris trajectories as functions of non-dimensionalization parameter l_c. The initial epoch for the ephemeris trajectory is fixed at Jan. 20 2023 00:00:00 UTC.

Several other CR3BP L_1/L_2 cycler orbits are transitioned to a SEM ephemeris model. The CR3BP initial guesses are plotted alongside their ephemeris counterparts in Figure 24. By leveraging appropriate characteristic parameters for each scenario, the transition strategy succeeds in preserving the geometry of even the most complex L_1/L_2 cycler orbits that possess several close Lunar passes and large out-of-plane amplitudes. The L_1-vertical-to-L_2-vertical cycler orbits in Figures 24(c) and 24(d), for example, possess mean periods of approximately 81 days, minimum perilunes of 31,000 km, and out-of-plane excursions up to 359,000 km. The regions that this trajectory passes through in a single period renders it especially susceptible to both Lunar and Solar gravity perturbations. Despite this sensitivity, the L_1-vertical-to-L_2-vertical cycler trajectory responds to the same transition strategy that is employed for the less complex halo-to-halo cycler in Figure 20. The other two geometries shown are also transitioned by employing this transition strategy. The ephemeris trajectories retain their structure when the initial epoch is varied across a full sidereal period in January of 2023.

SUMMARY

This investigation explores an alternative approach to identify natural structures that link the L_1 and L_2 regions. Previous authors offer a breadth of available natural structures connecting L_1 and L_2 Lyapunov orbits, but significant challenges exist in attempts to expand the methodology to the spatial case. By transforming known heteroclinic connections into periodic solutions, the methodology permits application of traditional orbit analysis tools, leading to the generation of orbit families and the expansion into the spatial problem via bifurcation and continuation strategies. These periodic trajectories produced with the cycler methodology display orbit-to-orbit transfer-like structures over a large range of energies and geometries, providing a large range for mission design options. Additionally, this methodology allows for augmentation of these L_1/L_2 cycler orbits such that extended revolutions in the vicinity of the equilibrium point of interest can address specific applications. The L_1/L_2 cycler orbits are validated in a higher-fidelity ephemeris model, and methodologies for ensuring geometry retention are key to constructing suitable ephemeris results. Adequate implementation

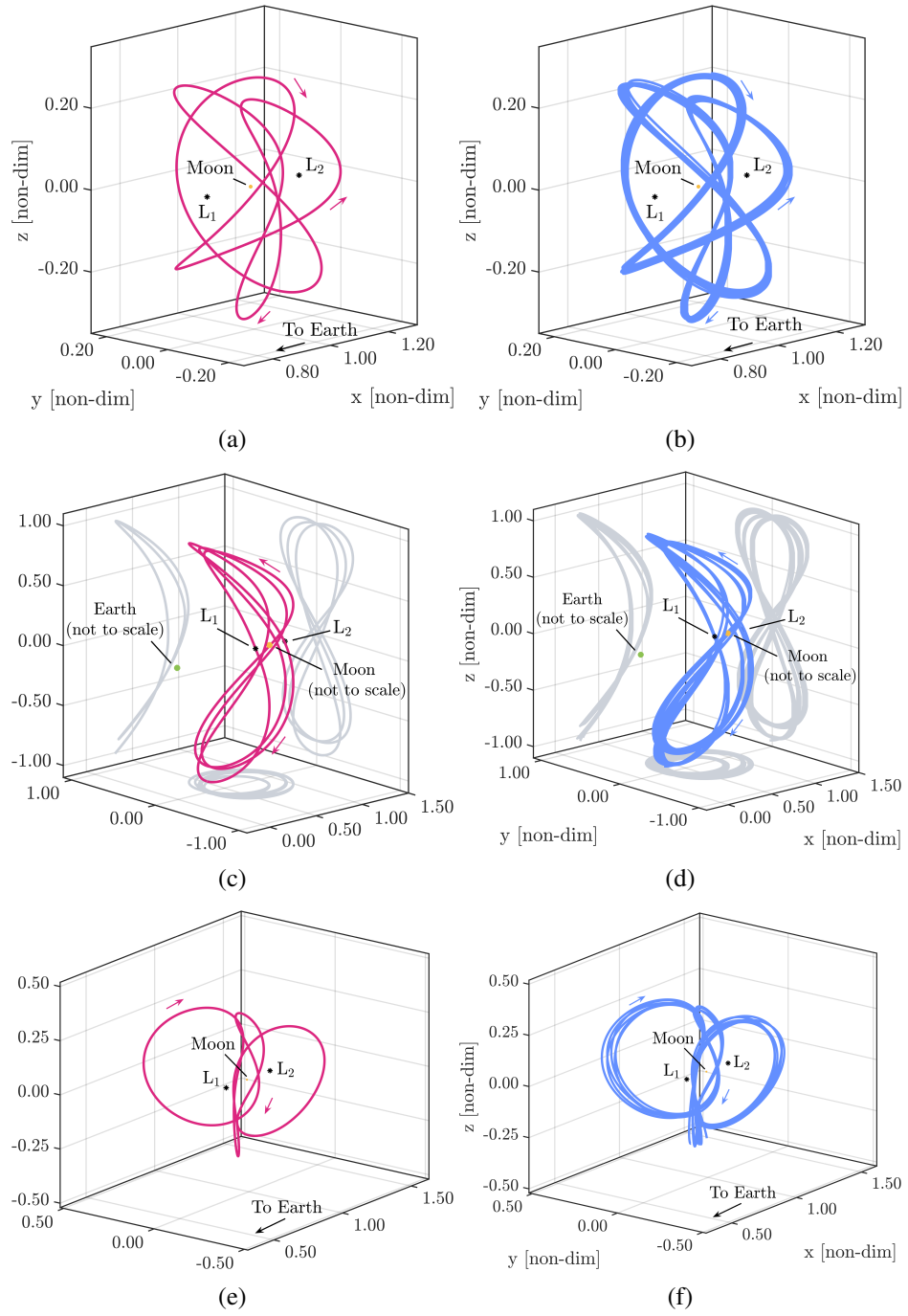

Figure 24: Comparisons of various CR3BP L_1/L_2 cycler orbits and two-year ephemeris counterparts. In each row of images, the red CR3BP initial guess is plotted alongside its blue ephemeris counterpart transitioned with an initial epoch is Jan. 20 2023 00:00:00 UTC.

of a numerical corrections scheme enables ephemeris transition for many cycler orbit geometries at any epoch.

ACKNOWLEDGEMENTS

The authors acknowledge the Aerospace Corporation for supporting this work under contracts PO 4600006951 and PO 4400000085. Beom Park is also acknowledged for his contribution of elliptical restricted three-body quasi-periodic orbits. Other members of the Multi-Body Dynamics Research Group also provided valuable discussions that furthered the work presented here.

REFERENCES

[1] "Moon Missions Exploration," https://moon.nasa.gov/exploration/moon-missions, 03 2023.

[2] W. S. Koon, M. W. Lo, J. E. Marsden, and S. D. Ross, "Heteroclinic connections between periodic orbits and resonance transitions in celestial mechanics," *Chaos: An Interdisciplinary Journal of Nonlinear Science*, Vol. 10, June 2000, pp. 427–469. http://www.cds.caltech.edu/ koon, 10.1063/1.166509.

[3] G. Gómez, W. S. Koon, M. W. Lo, J. E. Marsden, J. Masdemont, and S. D. Ross, "Connecting orbits and invariant manifolds in the spatial restricted three-body problem," *Nonlinearity*, Vol. 17, 05 2004, p. 1571, 10.1088/0951-7715/17/5/002.

[4] A. F. Haapala and K. C. Howell, "A Framework for Constructing Transfers Linking Periodic Libration Point Orbits in the Spatial Circular Restricted Three-Body Problem," *International Journal of Bifurcation and Chaos*, Vol. 26, May 2016, p. 1630013, 10.1142/S0218127416300135.

[5] D. Henry and D. Scheeres, "A Survey of Heteroclinic Connections in the Earth-Moon System," *73rd International Astronautical Congress*, No. IAC-22,C1,9,3,70258, Paris, France, 09 2022.

[6] D. C. Folta, M. Woodard, K. Howell, C. Patterson, and W. Schlei, "Applications of multi-body dynamical environments: The ARTEMIS transfer trajectory design," *Acta Astronautica*, Vol. 73, 2012, pp. 237–249.

[7] C. Ocampo, "An Architecture For a Generalized Spacecraft Trajectory Design and Optimization System," *Libration Point Orbits and Applications*, May 2003. pp. 529-571.

[8] V. Muralidharan and K. Howell, "Leveraging Stretching Directions for Stationkeeping in Earth-Moon Halo Orbits," *Advances in Space Research*, Vol. 69, 01 2022, pp. 620–646.

[9] C. H. Acton, "Ancillary data services of NASA's Navigation and Ancillary Information Facility," *Planetary and Space Science*, Vol. 44, Jan. 1996, pp. 65–70, 10.1016/0032-0633(95)00107-7.

[10] C. Acton, N. Bachman, B. Semenov, and E. Wright, "A look towards the future in the handling of space science mission geometry," *Planetary and Space Science*, Vol. 150, Jan. 2018, pp. 9–12, 10.1016/j.pss.2017.02.013.

[11] M. Vaquero, "Spacecraft Transfer Trajectory Design Exploiting Resonant Orbits in Multi-Body Environments," 2013. Ph.D. Dissertation, Purdue University, West Lafayette, Indiana.

[12] E. Canalias and J. J. Masdemont, "Homoclinic and heteroclinic transfer trajectories between planar Lyapunov orbits in the sun-earth and earth-moon systems," *Discrete and Continuous Dynamical Systems*, Vol. 14, No. 2, 2006, pp. 261–279, 10.3934/dcds.2006.14.261.

[13] K. Howell, B. Barden, and M. Lo, "Application of Dynamical Systems Theory to Trajectory Design for a Libration Point Mission," *Journal of the Astronautical Sciences*, Vol. 45, No. 2, 1997, pp. 161–178.

[14] A. Roy and M. Ovenden, "On the Occurrence of Commensurable Mean Motions in the Solar System: The Mirror Theorem," *Monthly Notices of the Royal Astronomical Society*, Vol. 115, 06 1955, pp. 296–309.

[15] R. Broucke, "Stability of periodic orbits in the elliptic, restricted three-body problem," *AIAA Journal*, Vol. 7, 1969, pp. 1003–1009, 10.2514/3.5267.

[16] E. Zimovan-Spreen, "Trajectory Design and Targeting for Applications to the Exploration Program in Cislunar Space," 2021. Ph.D. Dissertation, Purdue University, West Lafayette, Indiana.

[17] B. Park and K. C. Howell, "Leveraging Intermediate Dynamical Models for Transitioning from the Circular Restricted Three-Body Problem to an Ephemeris Model," *AAS/AIAA Astrodynamics Specialist Conference*, Charlotte, North Carolina, 2022.

[18] T. Pavlak and K. Howell, "Evolution of the Out-of-Plane Amplitude for Quasi-Periodic Trajectories in the Earth-Moon System," *Acta Astronautica*, Vol. 81, 2012, pp. 456–465.